

# Multistable Corrugated Shells

BY A. D. NORMAN, K. A. SEFFEN<sup>†</sup> AND S. D. GUEST

*Department of Engineering, University of Cambridge  
Trumpington Street, Cambridge CB2 1PZ, UK*

We have been constructing and investigating multistable corrugated shell structures. The multistability arises from the interaction between internal prestresses created during forming and non-linear geometrical changes during deformation. Using a simplified analytical elastic model, we homogenise the properties of the shells through simultaneously considering the material on two scales: the ‘local’ scale of the isotropic material and the ‘global’ scale of the corrugated sheet, which is then modelled as an equivalent flat sheet with anisotropic properties. This model is applied to simulate two modes of bistability observed in prototypes: first, prestressed corrugated shells which, when buckled, can coil up into a tube repeatedly and reversibly and, second, corrugated sheets with a symmetry-breaking ‘twisting’ curvature. The model gives an intuitive understanding of the behaviour, and has enabled us to understand forming processes that give the behaviour we wish, including tristable shells which combine both bistable modes.

**Keywords:** bistable, corrugated, morphing, multistable, prestress, shell structure

## 1. Introduction

Figure 1 shows a simple bistable corrugated shell, originally conceived by the second author and co-workers. It is made of an isotropic Copper-Beryllium (CuBe) alloy. One stable state, Fig. 1a, is a globally flat corrugated sheet which is not unstressed, for residual bending stresses attempt to coil the sheet. If part of the shell is manually flattened across the corrugations, these stresses are ‘released’, and the sheet coils up rapidly into the state in Fig. 1b. The shell can be repeatedly and reversibly ‘snapped’ between the two states, and at no point is the deformation plastic. This coiling/uncoiling will be referred to as the ‘Mode I’ bistability.

During the making of these shells, we noticed also that most prototypes exhibited an unexpected ‘twisting’ bistability in their corrugated form, making the sheets tristable, with no completely flat mode. This is shown in Fig. 2. The original single, flat corrugated mode has now split into two corrugated modes of equal global curvature, which are symmetrical about the axis of the corrugations. This twisting mode will be referred to as the ‘Mode II’ bistability. Where both modes are present, the shell is tristable with two twisted states and one coiled state: this is referred to as ‘Mode III’ behaviour. In all of this behaviour, the ‘mid-surface’ of the corrugated shells appears to have a uniform, developable curvature, and this assumption underpins the analysis in this paper. We create a simplified theoretical analysis based on simple underlying principles, and use this to explain the presence

<sup>†</sup> Corresponding author. Tel: +44 (0)1223 7 64137 Fax: +44 (0)1223 3 32662 E-mail: kas14@eng.cam.ac.uk

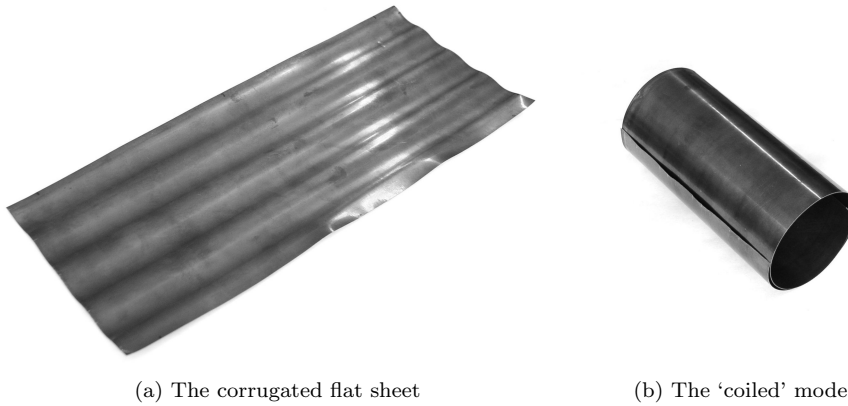


Figure 1: A typical shell exhibiting the 'Mode I' bistability, constructed from a conventional isotropic metal alloy (in this case, Copper-Beryllium). A bending prestress is held in equilibrium by the moment arm of the membrane stresses in the corrugated sheet (left): when the corrugations are elastically flattened, the prestresses are released and the sheet coils up.

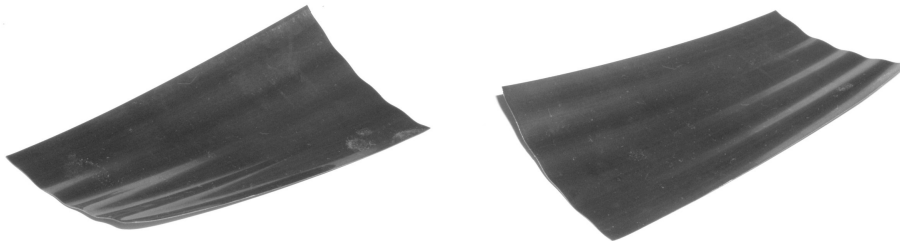


Figure 2: The two 'twisted' corrugated stable states of the 'Mode II' bistability. These Mode II stable states are in fact a cylindrical curvature of the corrugated sheet about an axis not aligned with the corrugations. When combined with Mode I, a tristable shell arises, referred to as 'Mode III'.

and behaviour of Modes I, II and III. Our model provides guidance on the forming processes to give shells that exhibit a particular behaviour.

*(a) Motivation and background*

Conventional structures are designed to maintain a single shape throughout their design life. Where a machine has to move to fulfil its function, we commonly see a series of such structures connected by hinges, linkages, sliders, bearings etc., both to provide and to constrain the degrees of freedom. Motion along these degrees of freedom is then directed by actuators, resulting in a complex system, requiring lubrication and maintenance.

‘Compliant’ structures are structures which undergo large deformations within their working life, typically remaining within the elastic limits of the material. Thus, they can undergo large changes of shape without hinges or mechanisms. If such a structure is also ‘multistable’, it can ‘lock’ into various shapes, giving the potential for large improvements in cost, weight, complexity, reliability and lifespan. Specifically, a *corrugated* shell structure can combine light weight with high strength, offering a wide scope for the designer to tailor the stiffness properties to the required behaviour.

Multistability has been observed in composite shells which are formed flat, but then distort as they are allowed to cool (Dano and Hyer, 1998). Cylindrical bistable shells, with two distinct shapes, have been studied by Kebabze et al. (2004) and Guest and Pellegrino (2006). These simple structures tend to have low stiffness, with a low energy penalty for slight changes in curvature magnitude and direction: they have a simple uniform cylindrical curvature. The corrugated shells here have a more complex shape and, hence, allow greater freedom in design; specifically, anisotropic properties can be produced through corrugation profiles, rather than through the use of anisotropic materials, as in Guest and Pellegrino (2006).

### (b) *Approach to manufacture and analysis*

The shells here are multistable because, in any given configuration, there are significant residual stresses, which are constrained by geometrical effects. When the shells are deformed in certain ways, these prestresses are ‘released’, leading to a dramatic change of shape as these stresses drive the rest of the transformation.

In prototypes, these stresses are deliberately caused during manufacture; the shell is plastically coiled, then elastically flattened in order to exert a bending stress throughout the shell, and finally plastically corrugated, which prevents the shell from coiling again. These two processes can be reversed in order. A material is required with sufficient hardness and ductility that the second working stage does not eradicate the stresses from the first; steels are suitable, but Copper-Beryllium alloy has been used here, due to the ease with which it can be hardened.

The layout of the paper is as follows. Section 2 develops an analytical model to simulate the general observed behaviour of the prototype shells. Section 3 then applies appropriate initial conditions and limits on deformation to predict and explain the three modes of multistability in terms of the principles upon which the analytical model of Section 2 is based. Finally, Section 4 presents conclusions and the new directions which this work provides. A full nomenclature is presented in Table 1.

## 2. Theoretical analysis

This section sees the development of a simplified model that separates the curvature of the shell into the ‘global’ or average curvature of the shell and the ‘local’ curvature of the corrugations themselves, which are assumed to be uniformly curved upwards or downwards.

The interaction of these two curvatures causes the shell to have local double curvature, so that during deformation, in addition to bending strains, there are significant stretching strains. However, a simple trick enables us to expedite simply

**Nomenclature**

$\theta$	Angle (degrees $^{\circ}$ )
$\kappa$	Curvature ( $\text{m}^{-1}$ )
$\lambda$	Corrugation wavelength (m)
$\nu$	Poisson's ratio
$\sigma$	Stress
$a$	Height of the corrugation above the mid-plane of the sheet at a point
$c$	Corrugation curvature ( $\text{m}^{-1}$ )
$k$	Global shell curvature ( $\text{m}^{-1}$ )
$t$	Local shell thickness
$w$	Absolute local out-of-plane distortion of the shell
$D$	Bending stiffness (N m)
$E$	Young's Modulus ( $\text{N m}^{-2}$ )
$M$	Bending moment per unit length (N)
$U$	Energy per unit area relative to an initial state ( $\text{N m}^{-1}$ )

**Subscripts, superscripts and operators**

$\overline{(\ )}$	Mean average over the material area/length
$(\ )_0$	Initial state
$(\ )_E$	Value at an equilibrium point
$(\ )_M$	Value at a local energy minimum (i.e. a stable point)
$(\ )_P$	Value at full plasticity
$(\ )_Y$	Value at yield
$\delta$	A small incremental change
$\Delta$	Change relative to a predefined initial state

**Dimensionless groups for Sections a and c**

$\hat{c}_0$	$c_0 t$
$\beta$	$c/c_0$
$\hat{k}$	$k/c_0$
$\hat{M}$	$-M/Dc_0$
$\hat{U}$	$\overline{U}/\frac{1}{2}Dc_0^2$

**Dimensionless groups for Section b**

$\check{k}$	$k/k_0$
$\check{M}$	$-M/Dk_0$
$\check{U}$	$\overline{U}/\frac{1}{2}Dk_0^2$

Table 1: Nomenclature

the consideration of stretching: the stiffness of the shell, in so far as it interacts with the *global* curvature, is modified to the anisotropic stiffness of the *mid-surface* of a corrugated shell. These effective mid-surface properties of a corrugated shell have a greatly increased bending stiffness in the direction of the corrugations relative to the local shell, and this increased stiffness accounts exactly for the stretching stresses. Note that the stiffness is actually orthotropic but the principle holds gen-

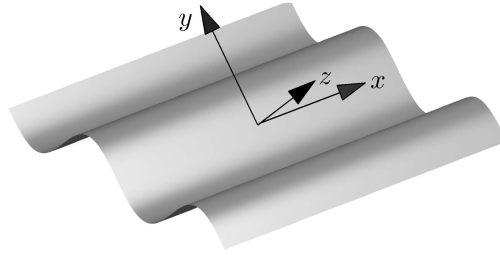


Figure 3: An intrinsic coordinate system is used, whereby  $z$  is always normal to the shell surface and  $x$  and  $y$  lie in the centreplane of the shell (and therefore vary in space), such that local  $z$ -direction displacement  $w$  and its first-order spatial derivatives must be zero, as outlined in Calladine (1983, chap. 2). The second-order spatial derivatives of  $w$  with respect to  $x$  and  $y$  give the shell curvature.

erally. Analysing corrugated shells through an equivalent orthotropic surface is a commonly used procedure; a recent historical review of this method is given by Liew et al. (2007).

In this process, some of these ‘global’ properties will depend on the local effects. The separation of these two scales gives the model its simplicity, and by attempting to capture the behaviour with a minimum complexity, we hope to infer meaningful insights on how they operate, without recourse to computational simulations.

(a) *Curvature*

The curvature of the shell is defined as follows:

$$\kappa_{xx} = -\frac{\partial^2 w}{\partial x^2} \quad \kappa_{yy} = -\frac{\partial^2 w}{\partial y^2} \quad \kappa_{xy} = -\frac{\partial^2 w}{\partial x \partial y} \quad (2.1)$$

where  $x$ ,  $y$  and  $z$  are a right-handed *intrinsic* coordinate system. Being intrinsic, this coordinate system varies over the shell such that  $x$  and  $y$  lie in the plane of the shell at any point, as in Calladine (1983, chap. 2), see Fig. 3.  $w$  denotes the displacement of the shell from the local  $x$ - $y$  plane in the  $z$  direction, and the basis vectors vary over the shell such that only second- and higher-order spatial derivatives of  $w$  with respect to  $x$  and  $y$  are non-zero. These equations are derived with the assumption that the material is thin relative to the radii of these curvatures and, given that this is true, this definition is valid for large deflections. While, in Section b, the stiffness of the *mid-surface* of the shell is considered for reasons elucidated above, the curvatures of Eqn 2.1 are in all cases local curvatures.

The shell curvature and shell bending moment *vectors* are defined as

$$\boldsymbol{\kappa} = \begin{bmatrix} \kappa_{xx} \\ \kappa_{yy} \\ 2\kappa_{xy} \end{bmatrix} \quad \mathbf{M} = \begin{bmatrix} M_{xx} \\ M_{yy} \\ M_{xy} \end{bmatrix} \quad (2.2)$$

where the  $x$  direction is aligned to the corrugations throughout.

A positive shell bending moment is defined such that the incremental increase,  $\delta U$ , in the stored strain energy due to the work done by moment,  $\mathbf{M}$ , over an

incremental change in curvature,  $\delta\boldsymbol{\kappa}$ , is given by

$$\delta U = \mathbf{M}^T \delta \boldsymbol{\kappa} \quad (2.3)$$

The ‘sense’ of a curvature refers to its sign: when two curvatures are in the ‘same’ sense, they are both positive or both negative in the  $z$  plane, and when they are in the ‘opposite’ sense, one is positive and the other negative. Note that this says nothing about their relative directions in the  $x$ - $y$  plane, but one physical interpretation is that the centres of their curvature lie above or below the shell.

(b) *Stiffness*

The shell material is assumed to be linearly elastic and to obey Hooke’s law with a Young’s modulus,  $E$ , and Poisson’s ratio,  $\nu$ . Furthermore, it is assumed that the shell can be modelled as being thin, leading to assumptions that, in bending, plane sections remain plane, shear stresses in the  $z$ -direction are negligible, and through-thickness stresses are zero.

The generalised Hooke’s law for the bending of an *isotropic* shell is given by Calladine (1983, chap. 2), where  $\Delta$  denotes the change from an initial state:

$$\begin{bmatrix} \Delta M_{xx} \\ \Delta M_{yy} \\ \Delta M_{xy} \end{bmatrix} = \Delta \mathbf{M} = \mathbf{D} \Delta \boldsymbol{\kappa} = D \begin{bmatrix} 1 & \nu & 0 \\ \nu & 1 & 0 \\ 0 & 0 & \frac{1}{2}(1 - \nu) \end{bmatrix} \begin{bmatrix} \Delta \kappa_{xx} \\ \Delta \kappa_{yy} \\ 2\Delta \kappa_{xy} \end{bmatrix} \quad (2.4)$$

where  $D$  is the flexural rigidity, defined by

$$D = \frac{Et^3}{12(1 - \nu^2)} \quad (2.5)$$

We now consider the stiffness of the corrugated sheet. Modelling the detail of the shell within the corrugations can be complex, but the goal here is to derive a simplified model involving the properties of the mid-surface of the corrugated shell. While the corrugations clearly have a large effect on the bending stiffness in the direction of the corrugations, the effect on other stiffness terms is much smaller, as shown by, e.g., Briassoulis (1986). Here, we assume that the corrugations only affect the bending stiffness in the direction of the corrugations. Thus, defining our axes so that the  $x$  direction is aligned to the axis of the corrugations, we assume the bending stiffness of the corrugated sheet in the  $y$  direction to be the same as the local value,  $D$ . In addition, the global twisting stiffness takes the local value,  $\frac{1}{2}(1 - \nu)D$ , and the Poisson coupling of curvature in the  $x$  and  $y$  directions remains at  $\nu D$ , as for the isotropic sheet. Only the bending stiffness along the corrugations is affected by the presence of the corrugations, and the local stiffness in that direction,  $D$ , is augmented by the moment-arm of the material about the central plane, giving an additional stiffness  $\alpha D$ , where  $\alpha$  is a function of the shape of the corrugations. This gives a new stiffness matrix

$$\mathbf{D} = \begin{bmatrix} (1 + \alpha)D & \nu D & 0 \\ \nu D & D & 0 \\ 0 & 0 & \frac{1}{2}(1 - \nu)D \end{bmatrix} \quad (2.6)$$

Our basic assumption is only valid if the equivalent mid-surface is developable, i.e. singly curved; any double curvature, or non-zero Gaussian curvature, would lead to stretching across the corrugations, which in turn has a significant effect on bending stiffnesses, and we would then need to couple bending with stretching in a strongly non-linear fashion. Note that  $\alpha$  is a variable during Mode I deformation as the corrugations flatten. This flattening of corrugations affects energy on a local scale within the corrugations, where the material is isotropic, and described by Eqn 2.4. This is pursued further in the coming section.

(c) *Energy*

This study of the behaviour of multistable structures involves finding stable equilibria. We follow the criteria for stability described by Guest and Pellegrino (2006):

1. for equilibrium, the local energy gradient, given by partial derivatives of total energy with respect to any shape factors, must be zero, and;
2. for stability, the stiffness matrix must be positive definite at that point, i.e. the structure must have positive stiffness in all modes of deformation away from the equilibrium shape.

Equilibria that do not fulfil the second criteria perform in one of three ways: either

1. all second-order derivatives are zero or negative: these are unstable points, and the structure may deform in any direction;
2. there are some negative second-order derivatives and some positive, so that the shape is unstable only in one direction, and stable in orthogonal directions; or
3. at least one second derivative is zero and none are negative, and the structure locally has zero stiffness: this is metastable behaviour.

These can all be found analytically, however, another method explores graphically the energy space around the equilibrium points, provided the number of independent variables is small: a stable state is then a minimum, while (1)-(3) are maxima, saddle points and troughs respectively.

If we define the change in curvature to be  $\Delta\boldsymbol{\kappa} = \boldsymbol{\kappa} - \boldsymbol{\kappa}_0$ , where subscript ‘0’ denotes the initial state, the elastic strain energy density at a given point for a given state is the integral of the work done,  $\mathbf{M}^T \delta\boldsymbol{\kappa}$ , over deformation from the initial state to that state. Therefore, the energy density  $U$  relative to the initial state  $(\boldsymbol{\kappa}_0, \mathbf{M}_0)$ , where  $\mathbf{M}_0$  is the shell’s stress state in its initial configuration, i.e. its ‘prestress’, is

$$U = \int_{\boldsymbol{\kappa}_0}^{\boldsymbol{\kappa}_0 + \Delta\boldsymbol{\kappa}} \mathbf{M}^T d\boldsymbol{\kappa} \quad (2.7)$$

$$= \int_{\boldsymbol{\kappa}_0}^{\boldsymbol{\kappa}_0 + \Delta\boldsymbol{\kappa}} \left( (\boldsymbol{\kappa} - \boldsymbol{\kappa}_0)^T \mathbf{D}^T + \mathbf{M}_0^T \right) d\boldsymbol{\kappa} \quad (2.8)$$

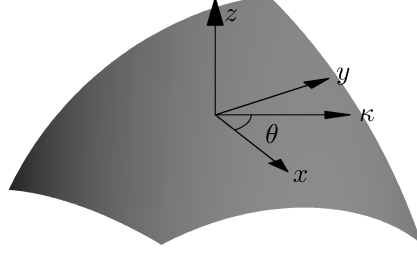


Figure 4: Definitions of the global cylindrical curvature  $k$  and its angle  $\theta$  to the  $x$  axis.

Noting that  $\mathbf{D}^T = \mathbf{D}$  and integrating,

$$U = \frac{1}{2} \Delta \boldsymbol{\kappa}^T \mathbf{D} \Delta \boldsymbol{\kappa} + \mathbf{M}_0^T \Delta \boldsymbol{\kappa} \quad (2.9)$$

This result and its derivation can also be found in Kebabze et al. (2004).

(d) *Combining the local and global scales*

We now divide the curvature of the corrugated shell into two components; the ‘global’ curvature vector, denoted by  $\mathbf{k}$ , and the corrugation curvature,  $\mathbf{c}$ .  $\mathbf{k}$  is the average curvature of the shell whilst  $\mathbf{c}$  is the local variation away from  $\mathbf{k}$  due to the corrugations themselves and so must average to zero over the sheet. The sum of these two curvatures is inserted into the strain energy density equation, Eqn 2.9, as outlined as follows.

Following Section b, only the global curvature  $\mathbf{k}$  is married to the additional stiffness  $\alpha D$ . Since  $\alpha D$  corresponds to the axis of the corrugations, it is perpendicular to the corrugation curvatures, which do not vary along the corrugations, and thus the only non-zero component of  $\mathbf{c}$  is  $c_{yy} = c(y)$ .

Furthermore, due to the assumption of inextensional behaviour, the global sheet is limited to a developable curvature, which is approximately uniform across the shell from observation. This curvature has some magnitude  $k$  in a direction making an angle  $\theta$  to the  $x$  axis, as shown in Fig. 4, and  $k$  and  $\theta$  are both constant over the shell. The global shell curvatures are then derived from a Mohr’s circle of curvature, as in Guest and Pellegrino (2006), to be

$$k_{xx} = \frac{1}{2}k(1 + \cos 2\theta) \quad k_{yy} = \frac{1}{2}k(1 - \cos 2\theta) \quad k_{xy} = -\frac{1}{2}k \sin 2\theta \quad (2.10)$$

Therefore, the total curvature is given as follows:

$$\Delta \boldsymbol{\kappa} = \mathbf{k} - \mathbf{k}_0 + \mathbf{c} - \mathbf{c}_0 \quad \mathbf{k} = \frac{1}{2}k \begin{bmatrix} 1 + \cos 2\theta \\ 1 - \cos 2\theta \\ -\sin 2\theta \end{bmatrix} \quad \mathbf{c} = \begin{bmatrix} 0 \\ c(y) \\ 0 \end{bmatrix} \quad (2.11)$$

where  $\mathbf{k}_0$  and  $\mathbf{c}_0$  are initial values. Note, again, that  $\alpha$  is a function of the corrugations, i.e. a function of  $c$ .

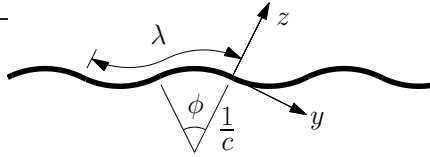


Figure 5: The circular-arc corrugation profile. The profile is repeated every wavelength,  $\lambda$ . The curvature has constant magnitude, but changes sign every half-wavelength; each half-corrugation is a circular arc subtending an angle  $\phi$ .

(e) *Corrugation profile*

Our prototype shells were constructed with circular-arc corrugations that repeat every wavelength  $\lambda$  (see Fig. 5). In addition to being simply made, this profile is expeditious in theoretical analysis, since the corrugation curvature  $c$  then has constant magnitude across the corrugations, swapping direction every half-wavelength. In other words, the initial corrugation curvature  $c_0(y)$  is

$$c_0(y) = \pm c_0 \quad (2.12)$$

where  $c_0$  is a constant. Each half-corrugation then subtends an angle  $\phi_0$ .

The deformed local curvature may not be uniform, but we make the simplifying assumption that, while the corrugations may be flattened out, they remain as circular arcs. We assume also that the  $\lambda$  does not change, i.e. the curvature  $c(y)$  is always in phase with the initial curvature  $c_0(y)$ . Thus, the corrugation curvature is always a simple multiple of the initial corrugation curvature, denoted by the coefficient  $\beta$ :

$$c(y) = \beta c_0(y) = \pm \beta c_0 \quad (2.13)$$

The initial corrugated shell has  $\beta = 1$ , and once the corrugations have been flattened and the sheet coils up,  $\beta = 0$ .

(f) *Limitations of the analysis*

The Mode I and Mode III analyses have a prestress moment which is entirely composed of a bending stress in the local sheet. In a corrugated sheet, there can also be a bending stress which is due to strains in the shell, but this, if it is present when the sheet is globally flat, implies that the sheet is not developable, and the corrugations can not therefore be flattened out. This form of bending stress can be present in the Mode II analysis since it does not require the corrugations to flatten out.

The  $\beta$  model of corrugation flattening described in Section e is simplistic: the corrugations are likely to flatten in a more complex fashion. As we are restricting possible modes of deformation, our results will give an upper bound on the moment at which the shell buckles. Also, note that edge effects are neglected throughout, on the assumption that they do not have a significant effect on the bulk behaviour.

### 3. Analytical model behaviour

The curvature defined in Eqn 2.11 has three terms that may be varied: global curvature magnitude  $k$ ; global curvature direction  $\theta$ ; and the function describing corrugation curvature,  $c(y)$ . This section considers the variation of:

1.  $k$  and  $c(y)$ , with  $\theta$  held at  $0^\circ$ , to describe the coiling Mode I bistability;
2.  $k$  and  $\theta$ , for the twisting Mode II bistability, where the corrugations do not flatten significantly;
3. and  $k$ ,  $\theta$  and  $c(y)$ , to model the tristable Mode III behaviour and also to determine stability conclusively, i.e. whether or not the stable points found in previous models are still stable when all other modes of deformation are present.

#### (a) Mode I: Coiling bistability

The global curvature of the shell is along the corrugations, in the direction in which stiffness is increased by  $\alpha D$ , so  $\theta = 0$ . Also, the initial state is chosen to be globally flat, with some prestress moment  $M_{xx0}$ , i.e. a prestress in the direction of the corrugations. This prestress is equivalent to having an externally applied moment. This initial state is undeformed, so there are no internal membrane stresses; it cannot, therefore, be in equilibrium with the bending prestress. However, we might expect equilibrium to be restored by only a small amount of curvature along the corrugations, producing the corrugated stable state observed in physical models.

Substituting the curvatures and prestress moments into Eqn 2.9 gives the strain energy density equation

$$U = Mk + \frac{1}{2}D \left\{ (1 + \alpha)k^2 + 2\nu k(1 - \beta)c_0(y) + [(1 - \beta)c_0(y)]^2 \right\} \quad (3.1)$$

This must be integrated over the entire sheet, but can be simplified. The sheet is assumed to be uniform, and hence to find the average energy density, we integrate Eqn 3.1 over one corrugation wavelength in the  $y$  direction and divide by the corrugation wavelength to find the average energy density over the sheet. No integration in the  $x$  direction is needed, since the curvatures do not vary along the corrugations. The average curvature of the shell in the  $y$  direction is the integral of  $c(y)$  over one wavelength  $\lambda$ , divided by  $\lambda$ . Since, in the initial state, the sheet has no global curvature in the  $y$  direction,

$$\frac{1}{\lambda} \int_0^\lambda c(y) dy = 0 \quad (3.2)$$

Both the  $Mk$  and the  $k^2(1 + \alpha)$  terms in Eqn 3.1 are constant over the shell; since, according to Eqn 3.2,  $c$  averages to zero, where the spatially-constant value  $2\nu k$  is multiplied by  $c$ , that term also vanishes. As  $\beta$  is assumed not to vary over the sheet, neither does  $(1 - \beta)^2$ , and thus the average strain energy density  $\bar{U}$  is revealed as

$$\bar{U} = Mk + \frac{1}{2}D \left[ (1 + \alpha)k^2 + \frac{(1 - \beta)^2}{\lambda} \int_0^\lambda c_0^2(y) dy \right] \quad (3.3)$$

From the corrugation profile described in Section e, the integral within Eqn 3.3 equals  $\lambda c_0^2$ . Dimensionless variables are introduced:

$$\hat{c}_0 = c_0 t \quad \hat{k} = \frac{k}{c_0} \quad \hat{M} = -\frac{M}{Dc_0} \quad \hat{U} = \frac{\bar{U}}{\frac{1}{2}Dc_0^2} \quad (3.4)$$

We choose to include the minus sign in the dimensionless group for moment so that we deal with positive values of  $\hat{M}$ :  $M$  itself will be negative because our model converts an internal prestress to an externally applied moment, and any prestress must be in the *opposite* sense to the resulting curvatures. Thus, by introducing the minus sign, moment-displacement plots such as Fig. 6 show positive stiffness when the structure is stable.

The dimensionless energy equation now reduces to

$$\hat{U} = \hat{k}^2(1 + \alpha) + (\beta - 1)^2 - 2\hat{M}\hat{k} \quad (3.5)$$

In order to calculate  $\alpha$  as a function of  $\beta$ , consider each element of length  $dy$  and thickness  $t$  to be a distance  $a$  from the centreplane of the corrugations, so that

$$\alpha D = \frac{1}{\lambda} \int_0^\lambda E a^2 t dy \quad (3.6)$$

This integral is soluble, giving

$$\alpha(\beta) = \frac{12(1 - \nu^2)}{\hat{c}_0^2} \left[ 1 + \frac{1}{2} \cos(\beta\phi_0) - \frac{3}{2\beta\phi_0} \sin(\beta\phi_0) \right] \quad (3.7)$$

$$\frac{d\alpha}{d\beta} = \frac{12(1 - \nu^2)}{\hat{c}_0^2} \left[ \frac{3}{2\phi_0\beta^2} \sin(\beta\phi_0) - \frac{3}{2\beta} \cos(\beta\phi_0) - \frac{\phi_0}{2} \sin(\beta\phi_0) \right] \quad (3.8)$$

which can be substituted back into Eqn 3.5. Equilibria are formally obtained by setting  $d\hat{U}/d\hat{k} = d\hat{U}/d\beta = 0$ , giving the following expressions for the equilibrium values, denoted by the subscript 'E':

$$\hat{k}_E = \frac{\hat{M}}{1 + \alpha_E} \quad (3.9)$$

$$\hat{U}_E = (\beta_E - 1)^2 - \frac{\hat{M}^2}{1 + \alpha_E} \quad (3.10)$$

$$\hat{M} = (1 + \alpha_E) \sqrt{2(1 - \beta_E) \left[ \frac{d\beta}{d\alpha} \right]_E} \quad (3.11)$$

Note that  $\beta_E$  is not given explicitly because there is no simple inversion of Eqns 3.7 and 3.8. Equation 3.11 can be inverted to give  $\beta_E$  in terms of  $\hat{M}$  by expanding the trigonometric terms in  $\alpha(\beta)$  into integer series, where the lowest-order terms cancel to zero and higher-order terms become negligible.

The equilibrium point found in Eqn 3.9 must be stable in  $k$ , as  $d^2\hat{U}/d\hat{k}^2 = 2(1 + \alpha) > 0$  for all shapes, but it might not be stable in  $\beta$ . This stability can be determined graphically from the generalised load-displacement plots, where a positive gradient equates to positive stiffness and stability but a negative gradient equates

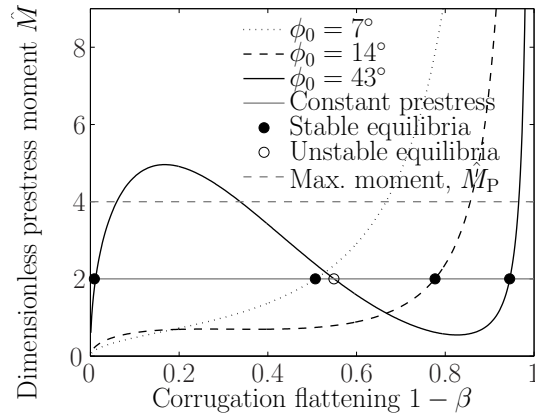


Figure 6: Equilibrium plot of moment  $\hat{M}$  against corrugation flattening  $1 - \beta$  at  $\hat{c}_0 = 6.25 \times 10^{-3}$ . The gradient of the equilibrium curve is the stiffness of the shell in flattening, so positive gradient = positive stiffness (stable) and negative gradient = unstable. A given prestressed shell has a constant  $\hat{M}$  (in this example, 2). Where the line of constant  $\hat{M}$  crosses the equilibrium curve, there is an equilibrium point. Below  $\phi_0 = 14^\circ$ , the unstable region vanishes and the structure becomes monostable. Also labelled is the maximum moment that CuBe alloy can provide,  $\hat{M}_P$ ; note that bistability is possible for moments well below it.

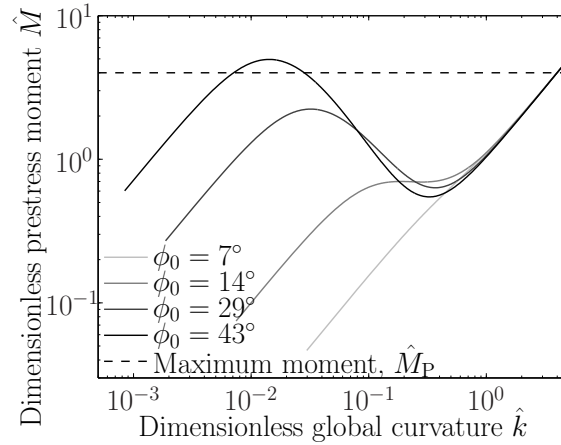


Figure 7: Log-log equilibrium plot of moment  $\hat{M}$  against global curvature  $\hat{k}$  at  $\hat{c}_0 = 6.25 \times 10^{-3}$ . Again, a given shell has a constant moment  $\hat{M}$ , and the equilibrium points for the shell are where the constant- $\hat{M}$  line crosses the equilibrium curve. This shows clearly the linear-elastic nature of the stable regimes, with the second stable state corresponding to the linear stiffness of an uncorrugated sheet. Also labelled is the maximum moment that CuBe alloy can provide,  $\hat{M}_P$ ; note that bistability occurs at moments well below it.

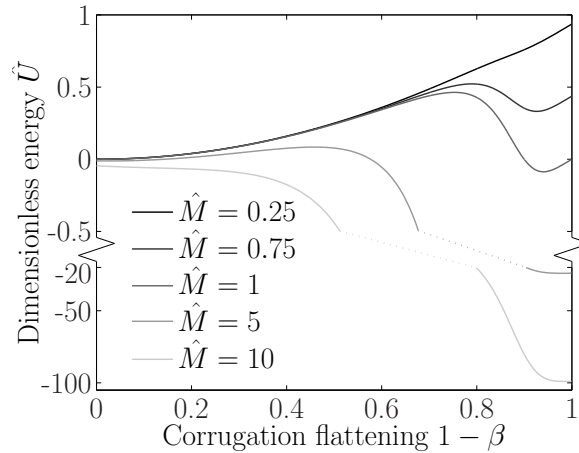


Figure 8: Plot of energy density relative to the initial state,  $\hat{U}$ , against corrugation flattening  $1 - \beta$  at  $\hat{c}_0 = 6.25 \times 10^{-3}$  and  $\phi_0 = 57^\circ$  for various moments  $\hat{M}$ . A large section of the  $\hat{U}$  axis has been cut out so as to give detail around  $\hat{U} = 0$  whilst showing features down to  $\hat{U} = -100$ . At higher  $\hat{M}$ , the coiled mode ( $\beta$  small) is lower-energy; at lower  $\hat{M}$ , the corrugated mode is lower-energy. For very large or small  $\hat{M}$ , the bistability vanishes.

to negative stiffness and instability. With Eqns 3.7-3.11, we can now describe the behaviour of the global and local curvature of the sheet under any moment  $\hat{M}$ .

Figure 6 plots Eqn 3.11, showing the equilibrium prestress moment  $\hat{M}$  related to the corrugation curvature  $\beta$ , for  $\hat{c}_0 = 6.25 \times 10^{-3}$ , which is chosen to match the physical shells where  $\hat{c}_0 = 50 \text{ m}^{-1}$  and  $t = 0.125 \text{ mm}$ . The gradient is the flattening stiffness of the shell in response to an applied moment: in this case, this moment is applied by the prestress, and is therefore fixed for a given shell. There are two regions of positive stiffness, between which there is one region of negative stiffness.

Given that  $\hat{M}$  is fixed for a specific shell, that shell is in equilibrium where the line of constant  $\hat{M}$  crosses the equilibrium curve, as given in example in Fig. 6 for an arbitrary value of  $\hat{M} = 2$ . We find that, for a range of values of  $\hat{M}$  for  $\phi_0 > 0.25$ , there are three equilibrium solutions for a given moment. Two of these lie on regions of positive gradient and are therefore stable; the point in between has negative stiffness and is unstable. Overall, these shells are bistable above a certain corrugation depth, for a range of moments. If the prestress moment is too low, there is no stable coiled mode, at low  $\beta$ ; if the prestress is too high, there will be no stable corrugated mode, at high  $\beta$ . In addition, as  $\phi_0$  becomes small, the corrugations tend to a flat sheet, which is not bistable.

Figure 7 shows the same data but plots  $\hat{M}$  against global curvature  $\hat{k}$ . This is the moment-curvature response of the shell, and its gradient is the bending stiffness of the shell. It can be seen that the corrugated stable form has very low global curvature. In the coiled mode, the moment-curvature relationship becomes linear with gradient  $D$ , or unity in our dimensionless form. In relation to a physical shell, it is important to ask whether this behaviour can be achieved within the elastic limits of the material. The precise nature of the internal stresses that produce the

moment is determined by the forming process history, but the maximum moment per unit length of shell that the material can sustain is the fully plastic moment,

$$M_P = \frac{1}{4}\sigma_Y t^2 \quad (3.12)$$

whose dimensionless magnitude is

$$|\hat{M}_P| = \frac{M_P}{Dc_0} = \frac{\sigma_Y}{E} \cdot \frac{3(1-\nu^2)}{\hat{c}_0} \quad (3.13)$$

For Copper-Beryllium alloy, the yield stress,  $\sigma_Y = 1200$  MPa, and Young's modulus,  $E = 131$  GPa, giving a dimensionless plastic moment  $\hat{M}_P \simeq 4$ . Figs 6 and 7 show that, for relevant values of  $\phi_0$ , bistability is possible with moments less than  $\hat{M}_P$ .

For bistable shells, if the shell is held such that half is coiled and the other half is corrugated, one of these states may have lower energy, in which case the transition region between them will move to the opposite end and the shell will globally take on the lower energy state. Fig. 8 shows the variation with  $\beta$  of the internal strain energy, relative to the strain energy at the initial state, for a range of moments at  $\phi_0 = 29^\circ$ ; note that the lower energy state is the corrugated state at low moment, but the coiled state at high moment. There is, therefore, one moment at which both states have approximately the same energy, and therefore any half-transformed shell will rest without becoming fully corrugated or fully coiled: it is 'neutrally stable', with no energy gradient in either direction. This feature occurs in Fig. 8 when  $\hat{M} = 0.88$ . It is reasonable that negative values of  $\hat{U}$  appear on Fig. 8, since the initial state of the sheet is not unstressed.

In summary, Fig. 9 shows the region of bistability. A simple algorithm produced the  $\hat{M}$ - $\beta$  curve for each combination of  $\hat{c}_0$  and  $\phi_0$ , and determined that that state was bistable if this curve had some local maximum and minimum that were not at  $\beta = 0$  and  $\beta = 1$ . This  $\hat{M}$ - $\beta$  curve was then transformed into a curve in two dimensionless groups such that the main determining factor for bistability becomes obvious. These groups were found by trial to correspond to the ratio of corrugation amplitude to material thickness, and to the ratio of corrugation amplitude to corrugation curvature radius. This provides a general design guide for the bistable shells.

### (b) Mode II: Twisting bistability

The shell has a prestress moment in the  $x$  direction as before. However, the corrugations are not permitted to flatten or buckle, i.e.  $\beta = 1$  at all times, but the global curvature is now no longer constrained to be in the  $x$  direction, i.e.  $\theta$  is allowed to vary.

Several specimens intended to display Mode I were also displaying Mode II. Observing this, it became obvious that, once the corrugated shell is given its prestress, a curvature across the corrugations appears, caused by the plastic forming process. This curvature is unstable in  $\theta$ , snapping to one of the two twisted modes. Therefore, in our attempt to model this bistability, we predicate a prestress moment  $M_{xx0}$  and an initial non-zero curvature  $k_0$  for  $\theta_0 = 90^\circ$ , i.e. *across* the corrugations.

Considerations of plasticity and the maximum moment permitted by the material are not relevant to this model since, first, the profile of the corrugations is

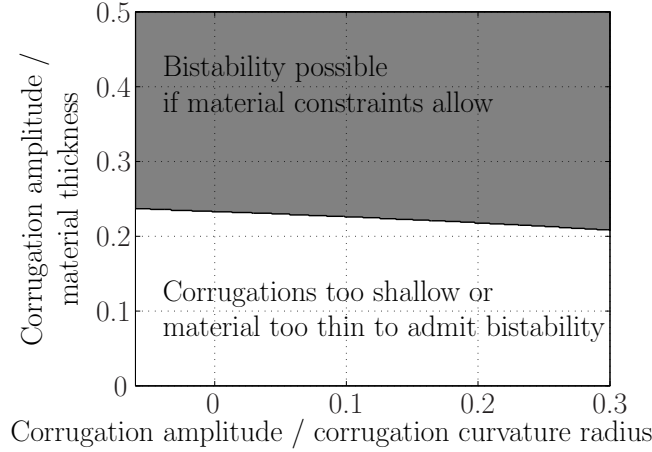


Figure 9: A design chart of the corrugation shapes over which coiling bistability is possible. On the  $x$  axis is the ratio of corrugation trough-to-peak amplitude to corrugation curvature radius, defined as  $2[1 - \cos(\phi_0/2)]$ , which is independent of the corrugation shape. The  $y$  axis gives the ratio of corrugation amplitude to material thickness, defined as  $2[1 - \cos(\phi_0/2)]/\hat{c}_0$ , which is purely a measure of corrugation shape, independent of material. As can be seen, bistability requires a corrugation amplitude at least 2 or 3 times the material thickness. Smaller corrugation radii, or tighter corrugation curvatures, also help bistability, but only very weakly.

irrelevant except in that they increase the stiffness by a factor  $\alpha$  and, second, since the corrugations need not be flattened out, the sheet is not constrained to be developable; this means that the prestress moment can consist not only of a shell bending moment but also of shell strains.

It is now convenient to make variables dimensionless against the initial curvature  $k_0$  rather than  $c_0$ . To contrast with Section a, these are denoted by ‘ $\checkmark$ ’:

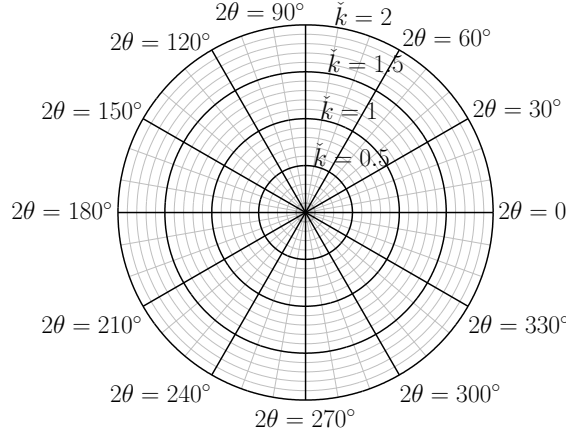
$$\checkmark k = \frac{k}{k_0} \quad \checkmark M = -\frac{M}{Dk_0} \quad \checkmark U = \frac{\bar{U}}{\frac{1}{2}Dk_0^2} \quad (3.14)$$

Equation 2.9 then becomes

$$\checkmark U = \checkmark k^2 \left[ 1 + \frac{\alpha}{8} (3 + 4 \cos 2\theta + \cos 4\theta) \right] + \checkmark k [(1 - \nu) \cos 2\theta - (1 + \nu)] + 1 - \checkmark M \checkmark k (1 + \cos 2\theta) \quad (3.15)$$

Equilibrium configurations are given by  $d\checkmark U/d\theta = 0$  and  $d\checkmark U/d\checkmark k = 0$ , and solutions are obtained in closed form as follows. Stability is separately assessed and recorded:

1.  $\checkmark k_E = 0$ ,  $\cos 2\theta_E = \frac{1+\nu+\checkmark M}{1-\nu-\checkmark M}$ , if  $\checkmark M < -\nu$ . This is not a stable solution;
2.  $\checkmark k_E = 1$ ,  $\theta_E = 90^\circ$ . This is the initial state, is an equilibrium point for all cases, and is only stable when  $\checkmark M < 1 - \nu$ ;

Figure 10:  $(\kappa, 2\theta)$  polar grid definition

3.  $\check{k}_E = 1$ ,  $\cos 2\theta_E = 2 \frac{\check{M}-1+\nu}{\alpha-1}$ . This solution only exists for  $1-\nu < \check{M} < \alpha+1-\nu$ , and is always stable. Note that since ‘ $\cos 2\theta$ ’ is a symmetric function, there is a symmetric pair of stable solutions;
4.  $\check{k}_E = \frac{\check{M}+\nu}{\alpha+1}$ ,  $\theta_E = 0$ . This always exists, but is only stable when  $\check{M} > \alpha+1-\nu$ .

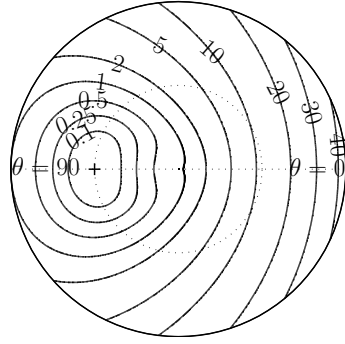
Henceforth, the values of  $\check{k}$  and  $\theta$  at stable equilibrium points are referred to as  $\check{k}_M$  and  $\theta_M$ , where the subscript ‘M’ denotes a value at a local energy minimum.

A contour plot of stored energy yields this information more intuitively. Stable equilibrium points are then evident as minima, and unstable equilibrium points appear as either maxima or saddle points. The two independent variables controlling the shape of the sheet are curvature magnitude and direction, and so a polar plot makes the most sense, as adopted by Kebabze et al. (2004). Figure 10 shows the plot coordinates: the distance from the origin denotes tightness of curvature  $\check{k}$  (so at the origin, the sheet is flat), while the angle on the plot denotes  $2\theta$ , rather than  $\theta$ , since curvature repeats every  $180^\circ$ .

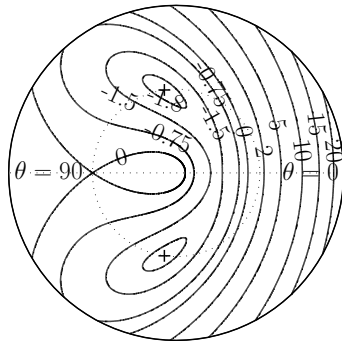
From the enumerated solutions above, there are three distinct modes of behaviour in which the stable points are located by different expressions. The bistable mode is found as solution (3), where  $\check{M}$  lies in the range

$$1 - \nu < \check{M} < \alpha + 1 - \nu \quad (3.16)$$

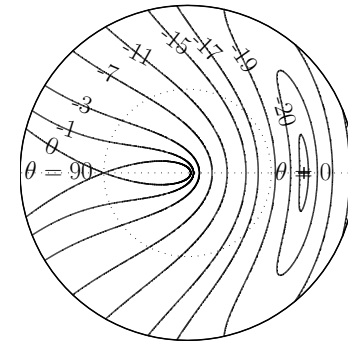
and only this range of prestress moments will provide bistability. For smaller or negative prestresses, there is just one stable point, at  $\theta = 0$ , which is solution (2), the initial state. For larger prestresses, the sole stable point is at  $\theta = 90^\circ$ , which is solution (4). Both of these solutions are present as saddle points on a bistable sheet. Fig. 11 shows all of this behaviour, giving contour plots of internal strain energy for a variety of prestress moments. As an aside, a negative  $\check{k}_0$  produces a bistability described by Kebabze et al. (2004), but this is not related to the Mode II twisting. Rather, the effect is that of a shell given two conflicting curvatures of perpendicular orientations of opposite sense, which are the two stable states.



(a) Monostable:  $\check{M} = 0$ , and so is too small for bistability, and the one stable point is at  $\check{k}_M = 1$ ,  $\theta_M = 90^\circ$ . There is a small saddle point at  $\check{k} = 0$ .  $\alpha = 10$



(b) Intermediate moments; two stable states at  $\check{k}_M = 1$ , at angle  $\pm\theta_M$  given by  $\cos 2\theta_M = 2(\check{M}-1+\nu)/\alpha-1$ . There are saddle points on  $\theta = 90^\circ$  (at  $\check{k} = 1$ ) and on  $\theta = 0$ .  $\check{M} = 5$ ,  $\alpha = 10$ .



(c)  $\check{M}$  has here been increased to 15, and bistability disappears.  $\theta_M = 0$ ,  $\check{k}_M > 1$ .

Figure 11: Energy-density contours for the two-dimensional model. Fig. 10 gives the  $(\kappa, 2\theta)$  polar grid definition for these plots. Contours are of energy  $\check{U}$  relative to the point  $\theta = 90^\circ$ ,  $\check{k} = 1$ , which is stressed, and therefore negative values are possible.  $\nu = 0.3$  throughout.  $\alpha = 10$  corresponds to  $\phi = 15^\circ$ , and  $\alpha = 145$  to  $\phi = 30^\circ$ . Crosses denote stable points (minima). Note that the  $\check{U} = 0$  contour crossing its own path in Figs 11b and 11c denotes a saddle point.

We have shown that the observed twisting behaviour can arise from the interaction between an initial curvature across the corrugations and a prestress moment along them. Equally, this can be seen as the result of two conflicting prestresses, and only arises when one prestress is not too much greater than the other; producing a two-dimensional prestress moment ( $M_{xx} \neq 0$ ,  $M_{yy} \neq 0$ ,  $M_{xy} = 0$ ) with  $k_0 = 0$  gives the same behaviour. Without the corrugations (i.e. in isotropic shells,  $\alpha = 0$ ), the range in Eqn 3.16 vanishes,  $\theta_M$  becomes indeterminate and the twisting bistabil-

ity becomes impossible to create. Note also that, once  $\alpha$  has been calculated, this behaviour is completely independent of the corrugation profile, and for a constant  $\alpha$ , triangular, sinusoidal, circular-arc or any other corrugation shape will behave identically. This is *not* true of the coiling bistability.

The final practical success of this model lies in its confirmation that the twisting bistability occurs when, due to plastic flow effects in manufacture, the shell acquires an unintended curvature across the corrugations. By plastically working this curvature out of the shell, the twisting modes can be eradicated.

(c) *Mode III: Tristability*

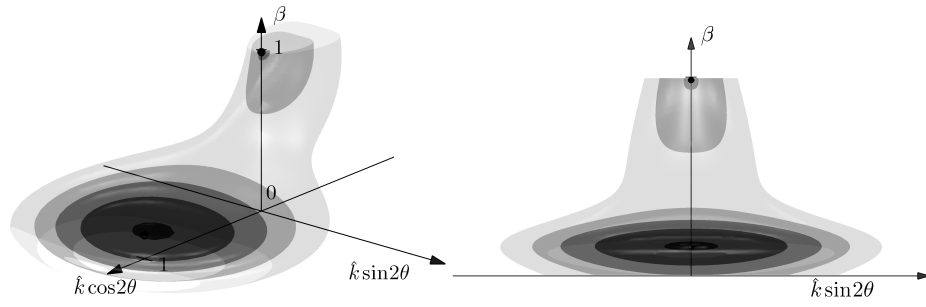
Allowing  $\kappa$ ,  $\theta$  and  $\beta$  to vary simultaneously provides a full model of the behaviour of the shells. The resulting model is more complex, but it captures the tristable behaviour of the combined Mode I and Mode II bistabilities. Rather than solving the equilibrium equations, we will plot the variation of stored energy with the three independent variables, using the dimensionless groups from Mode I, as in Eqn 3.17;

$$\hat{U} = \hat{k}^2 \left[ 1 + \frac{1}{8}\alpha(3 + 4\cos 2\theta + \cos 4\theta) \right] + \hat{k}\hat{k}_0[(1 - \nu)\cos 2\theta - (1 + \nu)] + \hat{k}_0^2 + (\beta - 1)^2 - \hat{M}\hat{k}(1 + \cos 2\theta) \quad (3.17)$$

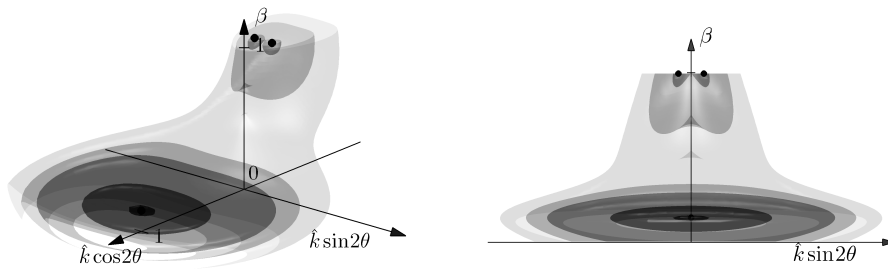
Graphically representing the variation of energy with three variables requires care. In the contour plots of Section b, each point corresponds to a unique shape in two variables ( $\hat{k}$ ,  $\theta$ ) which has a strain energy density. Adjacent points of identical strain energy density can be joined together to produce a contour line of constant  $\hat{U}$ ; each contour line, in Fig. 11, encloses a region of higher or lower energy than that contour, and therefore must enclose at least one maximum or minimum.

For three independent variables, the strain energy occupies a three-dimensional space, as shown in Fig. 12. The horizontal axes are the same as in Fig. 11, but there is also a vertical axis, representing corrugation amplitude  $\beta$  relative to the initial corrugation amplitude. Again, each point corresponds to a unique shape and has an associated energy. However, when points of identical  $\hat{U}$  are joined up, they now form a surface rather than a line, and that surface, again, encloses at least one maximum or a minimum. These surfaces are ‘isosurfaces’, i.e. surfaces over which the energy is constant. If a slice is taken through one of these plots, then a conventional contour plot results; if that slice is horizontal, the plots in Fig. 11 are produced.

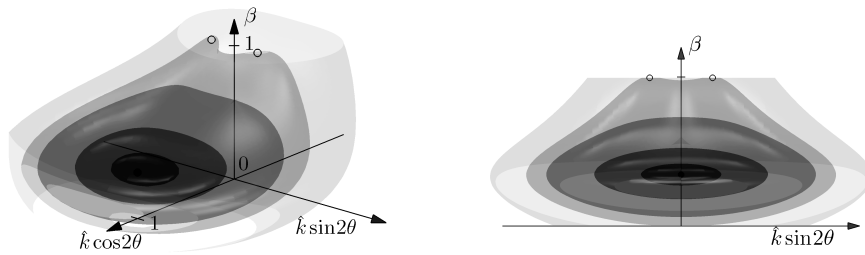
Three stable states do appear, each contained within an isosurface of low energy, and they are where we would expect to find them from the previous models. The previous models can therefore be expected to describe, qualitatively at least, the behaviour of tristable shells. Producing quantitative descriptions of the number and location of stable points for this three-dimensional model is complex. Most importantly, Fig. 12c demonstrates that a structure which appears to be bistable following the second elastic model can in fact be monostable when all three degrees of freedom are considered. This is a limitation only of the Mode II model, since the Mode I shell does not have the cross-corrugation curvature necessary for twisting bistability.



(a) The bistable Mode I, demonstrating that the stable points are also stable in  $\theta$ . Both are located in the  $\hat{k} \cos 2\theta$ - $\beta$  plane, as shown by the end-on view (right).  $\hat{k}_0 = 0$ ,  $\phi_0 = 29^\circ$



(b) A tristable shell. The coiled shape ( $\beta \sim 0$ ) is lower-energy.  $\hat{k}_0 = 0.2$ ,  $\phi_0 = 29^\circ$



(c) This demonstrates the value of the tristable model. The second model predicts this shell to be bistable when corrugation flattening is not allowed: the plane  $\beta = 1$  matches Fig. 11b, with ‘stable’ points marked by open circles. This plot shows these points to be not in equilibrium when the corrugations are circular-arc, and flattening (changes in  $\beta$ ) is allowed. There is a unique energy minimum, and the shell is monostable.  $\hat{k}_0 = 0.2$ ,  $\phi_0 = 14^\circ$ ,  $\hat{M} = 1$

Figure 12: 3-D energy isosurfaces for the ‘combined’ model. The coordinates are cylindrical polar: radius represents  $\hat{k}$ , angle represents  $2\theta$  and height  $\beta$ . Any point represents a global shape of the corrugated sheet. At this point, there is a certain value of internal strain energy density, and the surfaces on these plots are surfaces of constant energy. Filled black circles denote stable points. Darker surfaces are isosurfaces of lower energy.  $\hat{c}_0 = 6.25 \times 10^{-3}$  and  $\hat{M} = 1$  throughout.

#### 4. Conclusions and future work

Uniform corrugated shells can be manufactured which are bistable in either or both of two modes: a corrugated sheet which coils up when the corrugations are flattened, and a corrugated sheet which, in addition to curvatures along and perpendicular to the corrugations, has a ‘twist’ which is stable at both its positive and negative value. When these modes are combined in one shell, that shell is tristable. In both modes, multistability arises due to a ‘prestress’, i.e. a residual bending moment in the shell in the initial corrugated state which interacts with nonlinear changes in geometry.

We have delivered an elastic model, which evaluates the strain energy density of the shell as the shape is changed, in order to determine the stable shapes. Despite very simple assumptions of internal stresses, we have produced non-trivial results which reproduced a number of details of the behaviour of the prototypes. Furthermore, having produced these models, they have been sufficiently useful to guide our construction of prototypes, teaching us how to build in or eradicate specific modes of behaviour, and how to tailor the properties of the shells to suit the situation for which they are intended, which is one goal of shell-structure engineering.

We are grateful to Professor Emeritus C. R. Calladine FRS for insightful comments. Financial support from the EPSRC in the form of a research studentship for A.D.N. is gratefully acknowledged.

#### References

- D. Briassoulis. Equivalent orthotropic properties of corrugated sheets. *Computers & Structures*, 23(2):129–138, 1986.
- C. R. Calladine. *Theory of Shell Structures*. Cambridge University Press, 1983. ISBN 0521238358.
- M.-L. Dano and M. W. Hyer. Thermally-induced deformation behavior of unsymmetric laminates. *International Journal of Solids and Structures*, 35(17):2101–2120, June 1998. doi: 10.1016/S0020-7683(97)00167-4.
- S. D. Guest and S. Pellegrino. Analytical models for bistable cylindrical shells. *Proceedings of the Royal Society A: Mathematical, Physical and Engineering Sciences*, 462(2067):839–854, Mar. 2006. doi: 10.1098/rspa.2005.1598.
- E. Kebabze, S. D. Guest, and S. Pellegrino. Bistable prestressed shell structures. *International Journal of Solids and Structures*, 41(11-12):2801–2820, June 2004. doi: 10.1016/j.ijsolstr.2004.01.028.
- K. M. Liew, L. X. Peng, and S. Kitipornchai. Nonlinear analysis of corrugated plates using a fsdt and a meshfree method. *Computer methods in applied mechanics and engineering*, 196:2358–2376, 2007.